GEOPHYSICS, VOL. 71, NO. 2 (MARCH-APRIL 2006); P. V19–V30, 10 FIGS., 2 TABLES.
10.1190/1.2187799

Surface-consistent deconvolution using reciprocity and waveform inversion

Robbert van Vossen[1], Andrew Curtis[2], Andreas Laake[3], and Jeannot Trampert[1]

ABSTRACT

Source and receiver responses must be equalized when their behavior or coupling changes with location within a given survey. Existing surface-consistent deconvolution techniques that account for these effects assume that common-midpoint (CMP) gathering is valid — the seismic trace is decomposed into a source function, a receiver response, a normal-incidence reflectivity term, and an offset-related component that is laterally shift invariant. As a result, the performance of existing surface-consistent deconvolution techniques is best when applied to primary reflection data only, since the offset dependency of ground roll and multiples varies laterally in media with lateral variations.

We have developed an alternative method for surface-consistent deconvolution that is applicable to the entire seismic trace and is therefore essentially a raw-data preprocessing step. The method is based on reciprocity of the medium response. Assuming that conditions for applicability of reciprocity are met, we can attribute differences between normal and reciprocal recordings to the source and receiver perturbations. Contrary to existing surface-consistent deconvolution methods, this approach uses the full description of the wavefield and is therefore ideally suited for prestack processing.

We have applied this technique to single-sensor data acquired in Manistee County, Michigan. At this site, near-surface conditions vary, and this significantly affects data quality. The application of the new deconvolution procedure substantially improves S/N ratio on both prestack and poststack data, and these results compare favorably to those obtained using existing surface-consistent deconvolution techniques, since they require subjective data scaling to obtain acceptable results. The obtained source corrections are correlated to changes in near-surface conditions — in this case, to changes in water-saturation levels. We do not observe such a correlation for the receiver corrections, which vary rapidly along the spread. Finally, the receiver response does not agree with the generally accepted damped harmonic oscillator model. For frequencies below 100 Hz, the retrieved receiver variations are larger than predicted by this model, and we cannot explain the receiver response using a single resonant frequency for the geophone-ground coupling.

INTRODUCTION

The variability of recordings obtained in land seismic settings cannot be explained fully using linear wave propagation models because it partially depends on changes in source and receiver behavior within a given survey. For example, the source strength and signature mainly are determined by the material properties of the near-source region. As a consequence, the changing near-surface conditions deteriorate the so-called repeatability of the source (Karrenbach, 1994; Aritman, 2001). On the receiver side, several authors report discrepancies between signals recorded by geophones that are only a few meters apart (Berni and Roever, 1989; Blacquière and Ongkiehong, 2000). Some of the causes of these perturbations are imperfect geophone coupling, localized variations of the soil, shallow elastic property variations in consolidated rock, and variations of the ambient or recording equipment noise.

Detection and compensation for these perturbations are necessary in the early stages of processing, since the performance of multichannel filter operations rapidly deteriorates in the presence of amplitude or phase perturbations. This was recognized decades ago by Newman and Mahoney (1973), who demonstrate that the performance of the source and

Manuscript received by the Editor January 17, 2005; revised manuscript received August 9, 2005; published online March 10, 2006.
[1]Utrecht University, Department of Earth Sciences, Budapestlaan 4, 3584 CD Utrecht, The Netherlands. E-mail: vossen@geo.uu.nl; trampert@geo.uu.nl.
[2]Formerly Schlumberger Cambridge Research; presently The University of Edinburgh, School of Geosciences, Grant Institute, West Mains Road, Edinburgh EH9 3JW, United Kingdom. E-mail: andrew.curtis@ed.ac.uk.
[3]WesternGeco, Schlumberger House, Gatwick Airport, West Sussex RH6 0NZ, United Kingdom. E-mail: laakel@gatwick.westerngeco.slb.com.

receiver arrays is sensitive to source and receiver perturbations. These arrays, or more generally multichannel or frequency-wavenumber filters, are commonly used for ground roll and multiple attenuation. As indicated by Kelamis and Verschuur (2000), successful multiple elimination requires careful preprocessing of data.

Ideally, individual recordings are compensated for source and receiver perturbations before group forming. Therefore, storing recordings from individual receivers is recommended (Ongkiehong, 1988; Ongkiehong and Askin, 1988), which in principle allows the compensation for each individual geophone prior to digital group forming. Moreover, digital group forming is a reversible process, maintaining flexibility during the processing stages.

Source and receiver perturbations also could bias amplitude trends, such as amplitude versus offset (AVO); thus, successful compensation is essential for amplitude analysis (Castagna and Backus, 1993).

Even though compensation for acquisition effects should be done in the early stages of processing, existing surface-consistent deconvolution techniques assume that common-midpoint (CMP) gathering is valid (Taner and Koehler, 1981; Yu, 1985; Levin, 1989; Cambois and Stoffa, 1992; Cary and Lorentz, 1993) and therefore provides best results when applied to primary reflection data only.

In contrast, we use an alternative approach to compensate for source and receiver perturbations, which is essentially a preprocessing step. In principle, it can be applied directly to the recorded wavefield because it uses the complete seismic trace. Furthermore, it does not require midpoint binning, and no assumptions are imposed on the subsurface. The approach uses reciprocity of the medium response for evaluating lateral source and receiver amplitude variations. Assuming that conditions for applicability of reciprocity are met, differences between normal and reciprocal traces can be attributed to differences in source strength and receiver coupling. Karrenbach (1994) and Luo and Li (1998) apply this technique to determine the seismic source wavelet, assuming that the receiver perturbations can be neglected. Van Vossen (2005) demonstrates that the latter constraint is unrealistic and can be relaxed, adapting the procedure so that both source and receiver amplitude perturbations can be resolved.

Application of reciprocity requires symmetric data acquisition (Vermeer, 1991). This includes coincident source and receiver positions and shot/receiver patterns as well as identical source and receiver directivity. A field study performed by Fenati and Rocca (1984) indicates that, in practice, these reciprocal conditions need not be met exactly. They observe that the fit between normal and reciprocal traces is not influenced by the choice of a vibratory or explosive source, except at short offsets.

In this paper, we first review the source and receiver equalization procedure proposed and tested synthetically by van Vossen (2005). The main part of this paper is devoted to a field data application of the method. Data were acquired on a site in Manistee County, Michigan, which is characterized by changing near-surface conditions. Therefore, these data provide an excellent test case for the method. We discuss the characteristics of the source and receiver corrections obtained, and we show that these are correlated to the near-surface conditions. Furthermore, we show the influence of amplitude corrections on both prestack and poststack data and compare the results to those obtained with existing surface-consistent deconvolution techniques.

SOURCE AND RECEIVER DECONVOLUTION PROCEDURE

In this section, we briefly review existing surface-consistent deconvolution techniques and discuss the theoretical framework of the newly developed method.

Existing techniques and reciprocity

In the following, we consider single-component data and denote the vertical component of the recorded particle velocity by $v(t, \mathbf{x}_s, \mathbf{x}_r)$, with $\mathbf{x}_s$ and $\mathbf{x}_r$ the source and receiver positions, respectively. Considering the earth as a linear system for the propagation of seismic waves, the recorded traces satisfy the convolutional model

$$v(t, \mathbf{x}_s, \mathbf{x}_r) = R(t, \mathbf{x}_r) * G(t, \mathbf{x}_s, \mathbf{x}_r) * S(t, \mathbf{x}_s), \quad (1)$$

where $R(t, \mathbf{x}_r)$ is the receiver response, for the vertical component recordings at surface location $\mathbf{x}_r$; $S(t, \mathbf{x}_s)$ is the source signature at surface position $\mathbf{x}_s$, and $G(t, \mathbf{x}_s, \mathbf{x}_r)$ is the corresponding medium response. The asterisk $(*)$ denotes convolution in the time domain; $R(t, \mathbf{x}_r)$ and $S(t, \mathbf{x}_s)$ are surface consistent. This means that effects associated with a particular source or receiver remain constant throughout the recording time and affect all wave types similarly, regardless of the direction of propagation. The values $R(t, \mathbf{x}_r)$ and $S(t, \mathbf{x}_s)$ account for nonlinearity effects at the source and receiver. Thus, the source term also comprises the nonlinear response in the near-source field, which is referred to as the source coupling. For far-field recordings, it is realistic to assume that wave propagation is linear; hence, the convolutional model can be used.

The goal of surface-consistent deconvolution is to decompose the recorded data into their individual components, given by the convolutional model (equation 1). Since equation 1 exhibits more unknowns $[S(t, \mathbf{x}_s)$, $R(t, \mathbf{x}_r)$, and $G(t, \mathbf{x}_s, \mathbf{x}_r)]$ than data $[V(t, \mathbf{x}_s, \mathbf{x}_r)]$, assumptions are required to determine unique source and receiver responses. Existing techniques reduce the number of unknowns in equation 1 by decomposing the medium response into a normal-incidence reflectivity $Y(t, \mathbf{x}_m)$ and an offset component $D(t, \mathbf{x}_k)$:

$$G(t, \mathbf{x}_m, \mathbf{x}_k) \approx Y(t, \mathbf{x}_m) * D(t, \mathbf{x}_k), \quad (2)$$

where the midpoint coordinate $\mathbf{x}_m = (\mathbf{x}_s + \mathbf{x}_r)/2$, and the offset coordinate $\mathbf{x}_k = \mathbf{x}_s - \mathbf{x}_r$. This decomposition assumes CMP gathering to be valid (Cambois and Stoffa, 1992). Therefore, optimum results are obtained when the data contain primary reflections only; in media with lateral variations, the offset response for multiples and ground roll vary for each midpoint location.

The newly developed deconvolution technique requires data acquisition in a geometry that allows the use of apparently redundant recordings of reciprocal traces. Such a geometry requires symmetric wavefield sampling — that is, data acquisition using identical source and receiver samplings. This geometry is recommended by Vermeer (1991) to avoid processing artifacts as a result of asymmetric source and receiver sampling. In the current application, the reciprocity

theorem states that the medium response (or Green's function) is invariant when the source and receiver positions are interchanged (Knopoff and Gangi, 1959). Reciprocity of the medium response is expressed as

$$G(t, \mathbf{x}_s, \mathbf{x}_r) = G(t, \mathbf{x}_r, \mathbf{x}_s). \quad (3)$$

This identity requires that the source directivity response (radiation pattern) is similar to the receiver response for the vertical particle-velocity geophone. We outline the practical limitations of the use of reciprocity later in the Discussion.

Instead of using the decomposition of the medium response into normal-incidence reflectivity and an offset-related component, reciprocity of the medium response is used in the newly developed technique to decompose the recorded data. An important difference with existing methods is that this approach uses the full description of the wavefield.

Large differences between normal and reciprocal traces are commonly observed in the field (Fenati and Rocca, 1984; Karrenbach, 1994). Karrenbach (1994) and Luo and Li (1998) explain these differences by lateral variations in source behavior only, assuming that differences in receiver behavior are small. We demonstrate that the latter constraint should be relaxed, and we develop a procedure for compensating the recordings for lateral multicomponent source and receiver amplitude variations (van Vossen, 2005). In the following section we review the inverse procedure for estimating these corrections.

Formulation of the inverse problem

Let us consider an acquisition geometry with N coinciding source/receiver positions. The convolutional model and reciprocity result in a system of equations that constrains the individual terms in the convolutional model. Similar to surface-consistent deconvolution, we can formulate a linear inverse problem in the log/Fourier domain (Taner and Koehler, 1981; Cambois and Stoffa, 1992), where log denotes the natural logarithm. The log/Fourier transform $\tilde{X}(\omega)$ of a time function $X(t)$ is defined as

$$\tilde{X}(\omega) = \log\left[\int_{-\infty}^{\infty} X(t) e^{-i\omega t} \mathrm{d}t\right], \quad (4)$$

with the inverse transform

$$X(t) = \frac{1}{2\pi}\int_{-\infty}^{\infty} e^{\tilde{X}(\omega)+i\omega t} \mathrm{d}\omega. \quad (5)$$

Since convolution in the time domain is equivalent to summation in the log/Fourier domain, the convolutional model becomes in the log/Fourier domain

$$\tilde{V}(\omega, \mathbf{x}_s, \mathbf{x}_r) = \tilde{R}(\omega, \mathbf{x}_r) + \tilde{G}(\omega, \mathbf{x}_s, \mathbf{x}_r) + \tilde{S}(\omega, \mathbf{x}_s). \quad (6)$$

The real part of equation 6 describes the decomposition of the natural logarithm of the Fourier amplitude spectra into the source, receiver, and medium-response terms, whereas, the imaginary part of equation 6 gives the decomposition of the phase. In the following, we consider only the amplitude component of the problem.

When analyzing the system of equations, it is convenient to recast equation 6 in a matrix-vector form:

$$\mathbf{d}(\omega) = \mathbf{A}\mathbf{m}(\omega), \quad (7)$$

where $\mathbf{A}$ is the coefficient matrix, $\mathbf{m}(\omega)$ contains the unknown parameters in the log/Fourier domain, and the data vector $\mathbf{d}(\omega)$ contains the measurements of the wavefield $\tilde{V}(\omega, \mathbf{x}_s, \mathbf{x}_r)$ for all source and receiver positions. The model vector $\mathbf{m}(\omega)$ is partitioned into the individual components:

$$\mathbf{m}(\omega) = \begin{pmatrix}\mathbf{m}_G^T(\omega) & \mathbf{m}_R^T(\omega) & \mathbf{m}_S^T(\omega)\end{pmatrix}^T, \quad (8)$$

where $\mathbf{m}_G(\omega)$ contains the medium-response terms, $\mathbf{m}_R(\omega)$ the receiver terms, $\mathbf{m}_S(\omega)$ the source wavelets, and where T is the transpose operator. The coefficient matrix $\mathbf{A}$ is frequency independent, containing only ones and zeros. We give expressions for the structure of $\mathbf{d}(\omega)$, $\mathbf{m}(\omega)$, and $\mathbf{A}$ in Appendix A.

In this optimization procedure, we treat reciprocity of the medium response as an exact relationship. Instead of inserting the reciprocal equations 3 in the coefficient matrix $\mathbf{A}$, we directly reduce the number of unknown parameters in $\mathbf{m}_G(\omega)$ by explicitly substituting the reciprocal medium-response terms using equation 3. Since the number of unknowns is reduced, this approach is computationally favorable.

Furthermore, we can only solve for relative source and receiver differences. Consequently, we can impose a zero-mean constraint on the source and receiver terms without loss of generality.

Regularization criteria

Additional information is required to obtain a unique solution to the inverse problem. We use a criterion that minimizes variation in common-offset sections of the medium response (van Vossen, 2005). Prior information (or the reference model), denoted by $\mathbf{m}^0$, is included in the inverse problem defining a cost function:

$$Y = (\mathbf{A}\mathbf{m} - \mathbf{d})^T \mathbf{C}_d^{-1}(\mathbf{A}\mathbf{m} - \mathbf{d}) + (\mathbf{m} - \mathbf{m}^0)^T \mathbf{C}_m^{-1}(\mathbf{m} - \mathbf{m}^0), \quad (9)$$

where $\mathbf{C}_d$ is the data covariance matrix, which is a matrix with only nonzero diagonal elements, and $\mathbf{C}_m$ is the prior model covariance matrix. Its inverse, $\mathbf{C}_m^{-1}$, is a block-diagonal matrix and can be written in partitioned form:

$$\mathbf{C}_m^{-1} = \theta \begin{pmatrix} \mathbf{C}_{m_G}^{-1} & \mathbf{0} & \mathbf{0} \\ \mathbf{0} & \mathbf{C}_{m_R}^{-1} & \mathbf{0} \\ \mathbf{0} & \mathbf{0} & \mathbf{C}_{m_S}^{-1} \end{pmatrix}, \quad (10)$$

where $\mathbf{C}_{m_G}$, $\mathbf{C}_{m_R}$, and $\mathbf{C}_{m_S}$ are the covariance matrices describing prior information on the medium response, receiver, and source terms, respectively, and θ is the overall damping parameter. The smaller the value of θ, the more the model parameters are allowed to vary and the better the data can be explained.

The least-squares solution of equation 9 is found by setting the derivatives with respect to the model parameters equal to zero, given by (e.g., Tarantola, 1987)

$$\tilde{\mathbf{m}} = \left(\mathbf{A}^T \mathbf{C}_d^{-1} \mathbf{A} + \mathbf{C}_m^{-1}\right)^{-1}\left(\mathbf{A}^T \mathbf{C}_d^{-1} \mathbf{d} + \mathbf{C}_m^{-1} \mathbf{m}^0\right). \quad (11)$$

Prior information on the medium response can be obtained by minimizing variation in common-offset sections of the medium response. It follows from the convolutional model that insufficient corrections for the source and receiver variations result in perturbations of the medium response. This

causes larger variations in common-offset sections of the medium response. Thus, if we correctly retrieve these lateral source and receiver variations, the amplitude variations in the common-offset sections of the medium response are reduced to the minimum required by the data. We give the corresponding expressions for $\mathbf{m}_G^0$ and for $\mathbf{C}_{m_G}^{-1}$ in Appendix B.

To obtain a unique solution to the inverse problem, it is not necessary to provide prior information on the source and receiver terms, so we use

$$\mathbf{m}_R = \mathbf{0}, \quad \mathbf{C}_{m_R}^{-1} = \mathbf{0}, \tag{12}$$

$$\mathbf{m}_S = \mathbf{0}, \quad \mathbf{C}_{m_S}^{-1} = \mathbf{0}. \tag{13}$$

Alternative to the minimum variation criterion, we could have used energy criteria, minimizing energy differences between two adjacent common-source and common-receiver gathers, to regularize the inverse problem. These criteria are explained in detail by van Vossen (2005). Our choice for the minimum-variation criterion was based on synthetic tests. On synthetic data, best results were obtained using minimum variation as a regularization criterion.

APPLICATION TO MICHIGAN FIELD DATA

In this section we discuss a field data application of the method. First, we describe the characteristics of the data and outline the preliminary processing. Then, we describe the source and receiver terms received. Finally, we show the results of applying these corrections to prestack and poststack data.

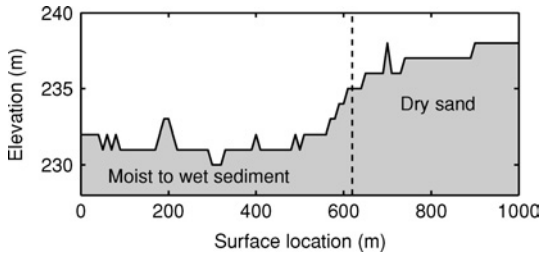

Figure 1. Surface topography and indication of near-surface material properties along the acquisition line.

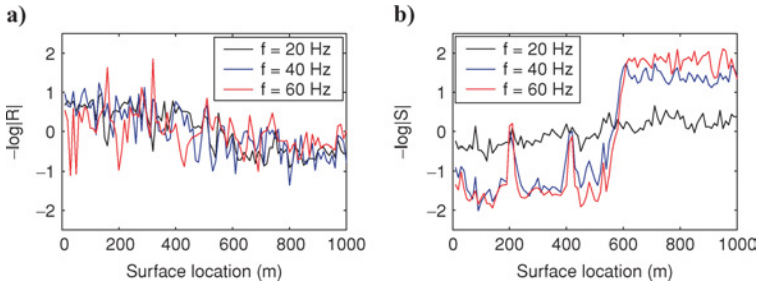

Figure 2. (a) Receiver and (b) source-amplitude corrections along the acquisition line for different frequencies. The logarithmic scale on the vertical axis denotes the natural logarithm.

Data description

We illustrate the method on 2D, single-sensor data acquired in Manistee County, Michigan. The site is characterized by changing near-surface conditions along the acquisition line. As indicated in Figure 1, near-surface conditions change from moist-to-wet sediments between 0 and 600 m to dry sands beyond that point (noted at time of acquisition). The location of the dry sands coincides with the more elevated sections along the acquisition line. Both source and receiver spacing is 10 m. The wavefield is emitted by an array of explosive sources located at approximately 1.5 m depth. The receivers are 10-Hz geophones. Furthermore, an important aspect of the acquisition is that each geophone is deployed at only one surface location, i.e.; the location of a geophone is fixed during the whole survey. The data set comprises recordings of 100 shots by 100 receivers.

The conditions for applying the deconvolution method are not exactly met. Small differences exist between source and receiver locations (on the order of a few meters), and the radiation pattern of the source array differs from the sensitivity kernel of the vertical component recordings. We assume that we can still treat reciprocity as an exact relationship for determining the source and receiver corrections. However, instead of directly using the inversion results for the medium-response terms $\mathbf{m}_G$, we use the lateral source and receiver terms to compensate the recorded data for these effects. By using only the source and the receiver terms, we do not force the data to be exactly reciprocal. We further assume that the source and receiver terms are minimum phase.

Thus, the equalization procedure consists of the following steps: First, we estimate the filters that compensate for lateral source and receiver variations in the log/Fourier domain for each frequency. Then, we apply the inverse log/Fourier transform and construct minimum phase filters. Finally, we compensate the recorded data for lateral source and receiver variations using spiking deconvolution (Yilmaz, 2001).

In principle, the deconvolution procedure can be applied directly to recorded data. We only perform trace editing to remove void records and to mute acausal noise generated by a pumping station in a few traces.

Characteristics of source and receiver corrections

As indicated by the synthetic experiments performed by van Vossen (2005), best results are obtained when the source and receiver terms are computed using a weak regularization term — that is, the minimum amount of regularization which yields a stable solution. The examples shown here are obtained using $\theta = 1$ (equation 10).

Figure 2 shows the correction terms for lateral source and receiver variations for the frequencies 20, 40, and 60 Hz. The receiver terms vary rapidly from point to point along the spread, whereas the source terms closely follow the changes in near-surface conditions (see Figure 1). Values larger than one correspond to corrections that increase the relative source strength, whereas values smaller than one indicate a relative energy decrease. Thus, a source located in the dry sand is strongly attenuated compared to a source in moist-to-wet sediments.

This can be explained by high-energy absorption rates and nonlinear deformation in the near-source region for a source located in the dry sand (Aritman, 2001). When sediments are water saturated, the compressibility dramatically changes, resulting in low-energy absorption rates close to the source.

Figure 3 shows the frequency dependence of the source corrections. For frequencies below 20 Hz, ground roll is dominant in the recordings. At these frequencies, the source corrections reflect not only the source coupling but also the success or failure of the source arrays to suppress ground roll. The smallest source corrections are obtained at $f = 20$ Hz. For higher frequencies, the behavior of the sources in the dry sand (for $x > 600$ m) clearly differs from the sources in the moist-to-wet sediments. The source is strongly attenuated in the dry sand, and this pattern is found for all frequencies higher than 25 Hz. Note that we solve only for relative source corrections, requiring that the average source correction is zero in the log/Fourier domain. Consequently, the shape of the average response curve in the dry sand resembles the negated average response curve for the sources in the moist-to-wet sediments.

Figure 4a shows four examples of the frequency dependence of the receiver corrections obtained in the inversion stage. The receiver corrections are smaller than the source corrections. Furthermore, the receiver corrections vary rapidly not only with offset but also with frequency. Limiting the impulse response in the time domain corresponds to a smoothing operation in the frequency domain. Figure 4b shows the effect of limiting the impulse response to 0.04 s. The shape of the correction filters above 125 Hz is the result of cosine tapers applied to avoid artifacts in the inverse log/Fourier transform.

Because we obtain only relative receiver corrections, we cannot compare these receiver corrections directly with the damped harmonic oscillator description, which is commonly used to describe geophone-ground coupling (Hoover and O'Brien, 1980; Krohn, 1984; see also Appendix C). However, we can compare ratios of the obtained corrections (differences in the log/Fourier domain) to ratios between two damped harmonic oscillators with different damping factors and resonant frequencies. Examples of differences of the retrieved receiver corrections are shown in Figure 4c, and the corresponding receiver locations are given in Table 1. Figure 4d shows differences between synthetic damped harmonic oscillator curves in the log/Fourier domain. The resonant frequencies and damping parameters are listed in Table 2. The spring of a geophone has typical resonance frequencies below 20 Hz (in this experiment, 10-Hz geophones were deployed), whereas the ground coupling for a vertical geophone is thought to resonate above 100 Hz (Hoover and O'Brien, 1980; Krohn, 1984).

The curves in Figure 4d are dominated by ground coupling with one bounded minimum and maximum value at high frequencies. The retrieved receiver corrections (Figure 4c) show different characteristics. Curves three and four have two distinct minima or maxima, while curves one and two have one bounded minimum and maximum, which qualitatively agrees with the damped-harmonic oscillator model. However, to explain curve two with this model, a 60-Hz resonant frequency is required, and this is much lower than the resonant frequencies reported for a vertical geophone (Hoover and O'Brien, 1980; Krohn, 1984). As a consequence, the damped-harmonic oscillator model only predicts significant perturbations in the high-frequency range, whereas the retrieved receiver corrections are large at lower frequencies as well. Thus, the retrieved receiver corrections cannot be explained with the damped-harmonic oscillator model using only one resonant frequency.

Results on prestack data

The effect of the equalization procedure on prestack data is illustrated in Figures 5 and 6, which show traces collected in

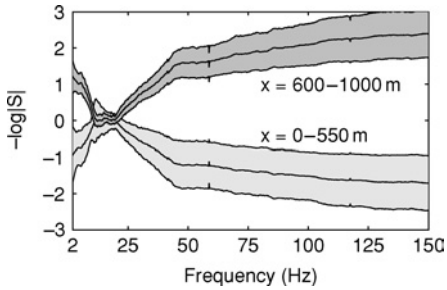

Figure 3. Source-amplitude corrections as a function of frequency. The average corrections are given for the source corrections in the intervals between 0 and 550 m and between 600 and 1000 m. The gray areas indicate the regions with at most one standard deviation difference with the average values.

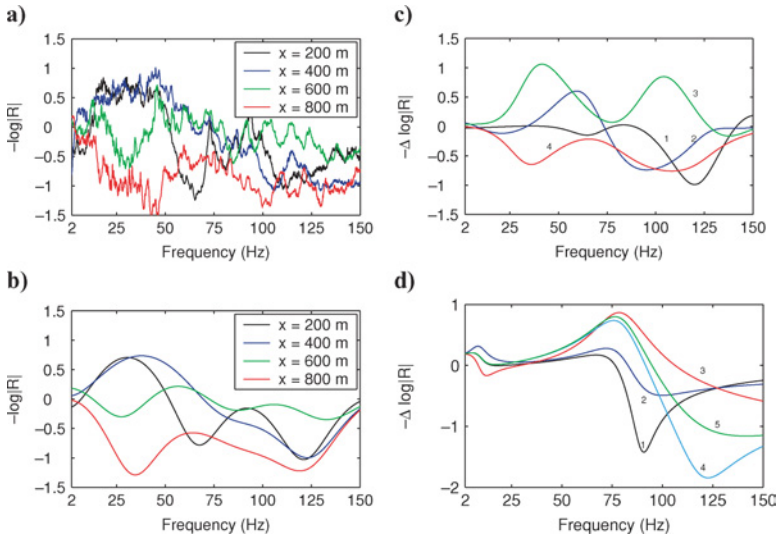

Figure 4. (a) Examples of obtained receiver-amplitude corrections at different locations. (b) Frequency response of these filters after limiting the impulse response to 0.04 s. (c) Differences between obtained receiver correction filters. The receiver positions corresponding to the labels are given in Table 1. (d) Differences between synthetic damped-harmonic oscillator-amplitude response curves. The resonant frequencies and damping factors corresponding to these curves are listed in Table 2.

a common-shot and a common-receiver gather with the common shot and common receiver located at $x = 100$ m. For visualization purposes, we apply offset scaling with the following function:

$$f(\mathbf{x}_o) = 1 + \eta \mathbf{x}_o, \tag{14}$$

with $\mathbf{x}_o$ the offset coordinate, $\eta = 0.10/\Delta x$, and Δx the source spacing (10 m).

The traces in the common-shot and common-receiver gathers have identical, uniform scaling. The differences between the traces in the gathers are evident. In the raw common-receiver gather (Figure 6a) the traces beyond $x = 600$ m generated by sources positioned in the dry sand (see Figure 1) are strongly attenuated. The corresponding reciprocal traces in the raw common-shot gather (Figure 5a) do not show such a signature of changing near-surface conditions. Another difference between the traces in the gathers is that correlated events are more pronounced in the near-offset section of the common-receiver domain.

Figures 5b and 6b show the data after correcting for the source and receiver perturbations. The common-receiver gather shows that reflectivity is measured beyond $x = 600$ m, indicating that we successfully correct for the source attenuation effect. Furthermore, in both common-receiver and common-shot corrected gathers, the correlated events are enhanced relative to the other energy.

The frequency-wavenumber (f–k) spectra corresponding to these data are shown in Figures 7 and 8. We compute these

Table 1. Locations of the receivers for which the obtained response ratio is plotted in Figure 4c.

Curve	Location 1 (m)	Location 2 (m)
1	200	210
2	400	410
3	600	610
4	800	810

Table 2. Corresponding receiver locations.

Curve	f_c (Hz)	η_c	f_g (Hz)	η_g
1	90	0.1	11.0	1.0
2	90	0.3	11.0	1.2
3	90	1.0	11.0	0.8
4	120	0.2	11.0	1.0
5	120	0.5	11.0	1.0

Parameters corresponding to the ratios of synthetic damped-harmonic oscillator geophone response curves given in Figure 4d. Parameters are varied for the geophone response in the denominator. The response curve in the numerator has the parameters $f_C = 80$ Hz, $\eta_C = 0.3$, $f_g = 10$ Hz, and $\eta_g = 1.0$. Variables are explained in Appendix C.

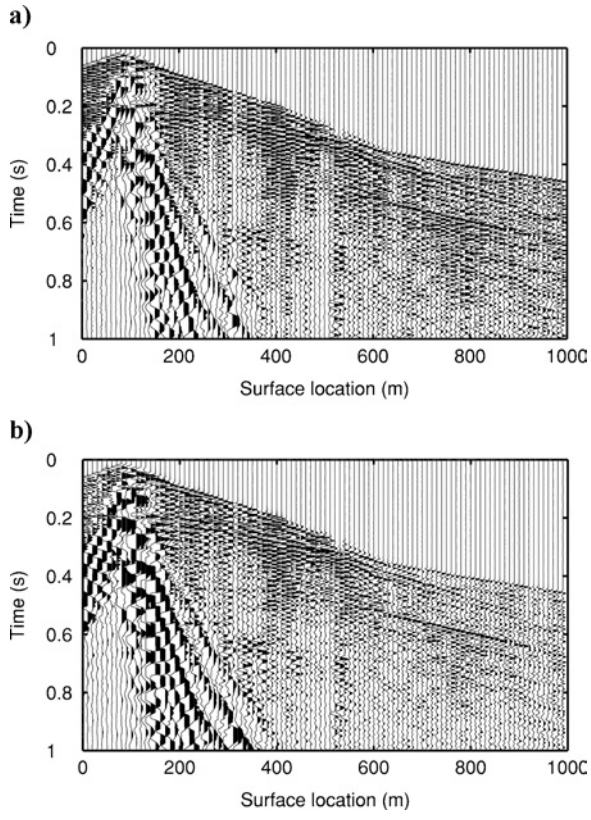

Figure 5. Effect of source- and receiver-amplitude corrections on a common shot gather for a source located at position $x = 100$ m: (a) input data; (b) filtered data. Both plots are scaled with respect to their maximum value (plotted with a similar relative amplitude scaling).

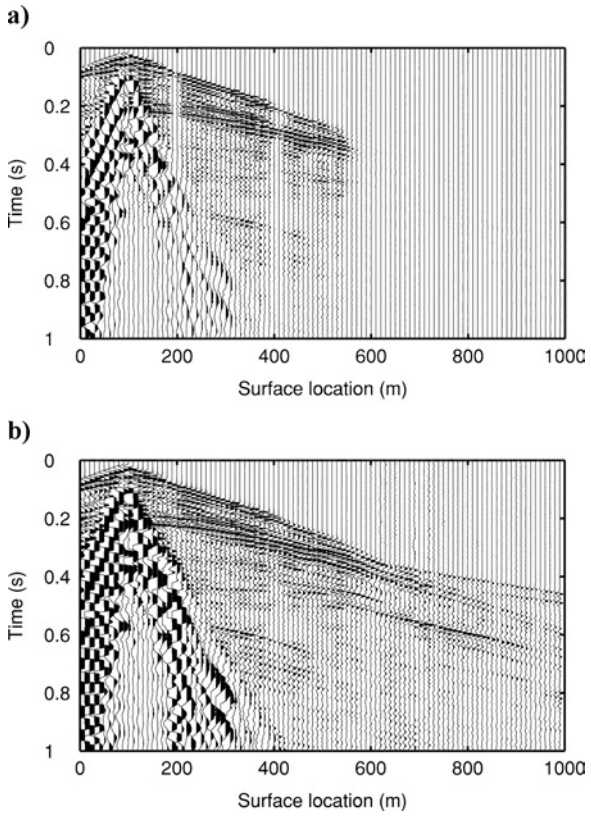

Figure 6. Effect of source- and receiver-amplitude correction on a common receiver gather for a receiver located at position $x = 100$ m: (a) input data; (b) filtered data. The plots are scaled similarly to the common-shot gather in Figure 5.

spectra using traces between 100 and 1000 m and then apply tapering at the edges of the domain to reduce artifacts. By selecting these traces, we can interpret energy corresponding to negative wavenumbers as noise. For the common-shot gather, the source corrections operate only along the frequency axis, whereas the receiver corrections operate along both the frequency and wavenumber axes. To assess the consequences of both source- and receiver-amplitude corrections, we first apply the receiver corrections (Figure 7b) and then the source corrections. The final results are shown on similar absolute (Figure 7c) and relative (Figure 7d) scaling to the original spectrum. These spectra suggest that we have more correlated energy after the source and receiver corrections relative to other energy, and we observe that the signal bandwidth and resolution increase in the common-receiver domain, e.g., compare the relative signal strength below 50 Hz between Figures 8a and 8d.

Figures 5b and 6b show that significant differences remain between normal and reciprocal traces. The spectra in Figures 7d and 8d indicate that source and receiver phase corrections could further improve the fit between normal and reciprocal traces, especially in the common-shot domain. Figure 2 shows that the receiver amplitude corrections vary erratically along the spread. Figure 7d suggests that the receiver phase perturbations also follow this pattern; this could explain the backscattered noise in this spectrum.

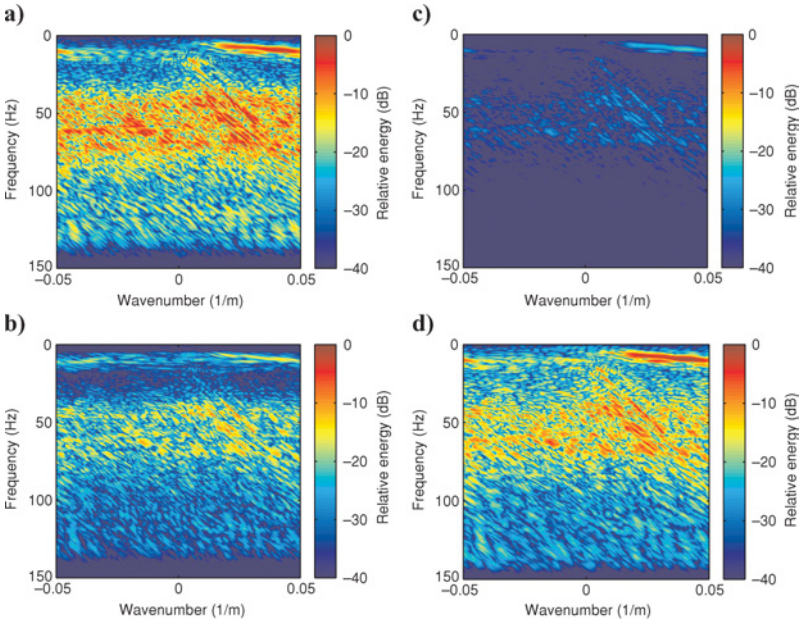

Figure 7. The *f-k* spectra of data shown in Figure 5 on a decibel scale (common-shot gather): (a) input data, (b) filtered data using only the receiver corrections, (c) filtered data using both source and receiver corrections. (d) Data displayed in (c) scaled with respect to its maximum value, whereas (a), (b), and (c) have identical scaling.

Results on poststack data

We finally evaluate the consequences of the applied source and receiver corrections on poststack data. The basic stacking sequence includes the following steps: (1) trace editing; (2) mute ground roll, air blast, and refractions (performed in the common receiver domain); (3) spherical divergence correction; (4) NMO correction; and finally (5) CDP stack. The poststack data are shown in Figure 9a, and the data which are compensated for lateral source and receiver differences between steps 1 and 2 are shown in Figures 9b, c. Shown are results obtained with data corrected for source perturbations only and with data corrected for both source and receiver perturbations. These stacks have similar scaling with respect to their maximum amplitudes. The right part of the sections is dominated by low-frequency events which are images of guided waves.

A comparison between the poststack data shows that the spurious dipping structures have been attenuated. These structures are associated with near-surface complexities, including source and receiver perturbations and statics. Because we did not apply static corrections before stacking the data, these spurious dipping structures have not been completely removed in Figure 9c. We also observe that reflectors are more continuous and can be more

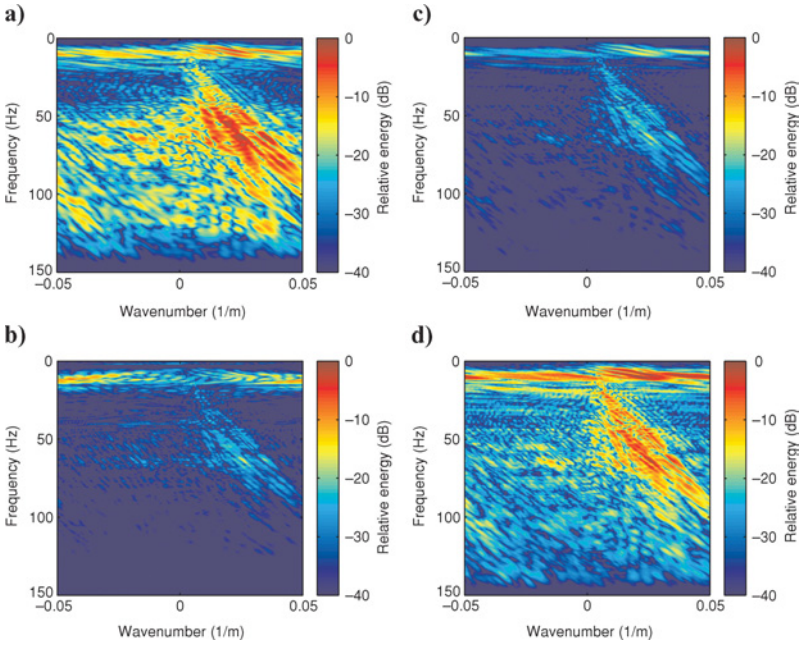

Figure 8. The *f-k* spectra of data shown in Figure 6 on a decibel scale (common-receiver gather): (a) input data, (b) filtered data using only the source corrections, (c) filtered data using both source and receiver corrections. (d) Data displayed in (c) scaled with respect to its maximum value, whereas (a), (b), and (c) have identical scaling.

easily identified. Thus, the new deconvolution procedure clearly improves the S/N ratio, and it demonstrates that both source and receiver perturbations must be taken into account.

Figure 9d shows poststack results after conventional surface-consistent deconvolution without using our new method. This has been applied to the data between steps 4 and 5. Clearly, there remains a signature of the source perturbations in these data; we attribute this problem to the damping of the source and receiver terms, which is applied in surface-consistent deconvolution to solve the nonuniqueness of the decomposition (e.g., Cambois and Stoffa, 1992). The source and receiver terms are assumed to be small. Therefore, we also apply surface-consistent deconvolution after increasing the source strength in all traces in common-shot gathers with sources located in the dry sand. These poststack results are shown in Figure 9e.

The poststack results in Figure 9 give a good first impression on the performance of the different deconvolution methods. We can make a few observations when comparing Figures 9c–9e. First, the reflectors in the central part of the section are better imaged in Figure 9c. Compare, for example, the image of the reflector at 0.8 s. Second, the signature of coherent noise, such as guided waves in the right part of the section, is less evident in Figure 9e. However, we cannot base a judgment on this last observation, since we expect that techniques which aim to suppress effects of coherent noise in the prestack domain also will benefit from the corrections obtained with the newly developed technique. Furthermore, we expect also that the conventional surface-consistent deconvolution techniques will benefit from removing coherent noise prior to the application. Thus, to assess the influence of coherent noise on CDP stacked data, the effectiveness of the suppression of different types of coherent noise needs to be investigated. This would require a comparison of fully processed data.

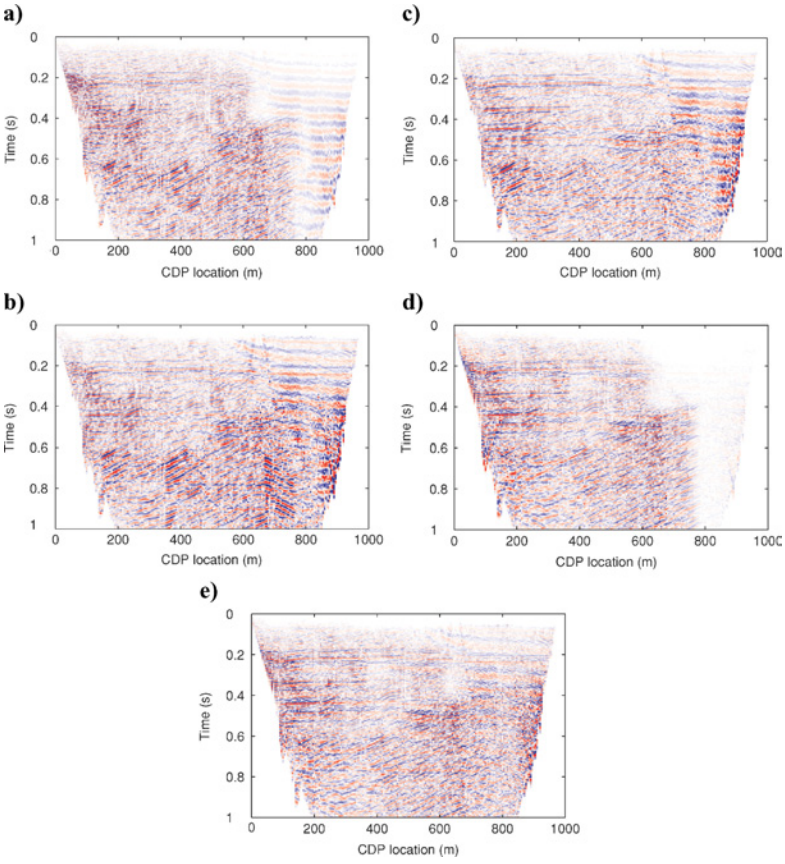

Figure 9. The effect of source and receiver equalization on CDP stacked data. (a) Uncorrected data, (b) data corrected for source perturbations only, (c) data corrected for both source and receiver corrections, (d) results obtained with existing surface-consistent deconvolution techniques, and (e) results obtained with existing techniques after increasing the source strength for sources located in the dry sands.

DISCUSSION

A critical assumption in our method is that we assume the conditions for applicability of reciprocity can be met. However, there are limitations in practical situations. First, the seismic source is strong enough to excite nonlinear wave-propagation effects in the near-field. Hence, in this region the convolutional model and reciprocity cannot be used to decompose the seismic trace into its individual components. Nevertheless, it is realistic to assume that wave propagation is linear in the far-field, implying that we can use the convolutional model and reciprocity. Second, in practice it is impossible to acquire data with exactly similar source and receiver locations. The influence of these positional differences can be minimized using parallel source and receiver lines at a close distance. In the data considered in this paper, the difference between source and receiver positions is smaller than 2.0 m. Furthermore, the source directivity or radiation pattern usually deviates from the sensitivity kernel of the receiver component considered — in this case, the vertical component. For example, if the ground is undulating, then it might be difficult to satisfy reciprocity when the truly vertical geophone at $\mathbf{x}_r$ is planted in a gently dipping hillside while on a neighboring steep hill the vibroseis truck has a plate parallel to the slanted ground. However, in vertically inhomogeneous media, i.e., in media that do not vary laterally, variations between the source radiation pattern and receiver response will not influence the performance of the method.

Strongly related to the radiation pattern of the source is the assumption that the source and receiver corrections are stationary for the whole seismic trace. This implies that the same corrections apply both to ground roll and reflection data, whereas these wave types originate from entirely different parts of the radiation pattern. Therefore, we expect that the optimum corrections for ground roll and reflection data will differ. This problem can be circumvented easily using the following approach. First, corrections can be computed using the whole seismic trace. It is realistic to assume that ground roll is dominant in the lower frequency range, so the low-frequency source and receiver terms apply primarily to ground roll. Then we can apply these

corrections to the data and suppress the effects of ground roll. Next, we can use the deconvolution method to recompute the corrections for the reflection data only.

Note that we use reciprocity as an optimization criterion to determine source and receiver amplitude perturbations. By compensating the recorded data for the source and receiver perturbations, we actually minimize differences between normal and reciprocal traces while still fitting the data. Since we do not use the inversion results for the medium response, we do not force the medium response to be exactly reciprocal, which in practical situations is unfeasible.

We assess the improvement of fit between normal and reciprocal traces comparing the amplitude of the envelope (Taner et al., 1979) before and after the deconvolution procedure. We quantify the relative differences using a relative L_2 norm as a measure:

$$\xi = \left\{ \frac{\sum_{t=0}^{N_t \Delta t} [A_n(t) - A_r(t)]^2}{\sum_{t=0}^{N_t \Delta t} [A_n(t) + A_r(t)]^2} \right\}^{1/2}, \qquad (15)$$

where $A_n(t)$ is the amplitude of the envelope of a normal trace, $A_r(t)$ denotes this for the corresponding reciprocal trace. We compute ξ for all reciprocal trace combinations in the survey and take the average value for each offset. Killed traces are not taken into account. Figure 10 shows ξ as a function of offset before and after the application of the equalization method. The fit between the envelope of normal and reciprocal traces significantly improves, except for short offsets. This is expected because wave propagation is nonlinear in this region.

We illustrate the application of this method on a relatively small data volume. For larger volumes, processing can be done in subsets — for example, groups of 100 identical source and receiver positions. Two adjacent groups can be best arranged such that these have a few sources and receivers in common. Then, the differences between the relative source corrections at these positions can be used to compute a transfer function between groups. This transfer function allows scaling of the relative source correction terms of the different subsets with respect to the same absolute reference value. The relative receiver terms can be scaled in a similar fashion. As a consequence, the equalization procedure is not restricted to a small 2D acquisition geometry. Also, 3D applications are possible, but this still requires an approximation to identical source and receiver sampling.

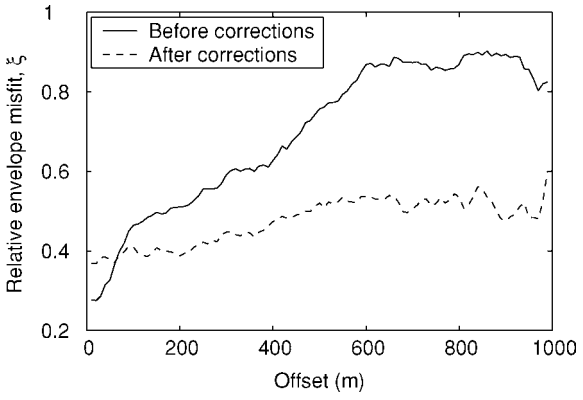

Figure 10. Envelope amplitude misfit as a function of offset before and after amplitude corrections. The misfit is computed using the first 3 s of the recorded signal.

For a regular recording geometry, the equalization procedure can be performed in real time in the field. This is a result of the characteristic that the coefficient matrix $\mathbf{A}$ (equation 7) is independent of the recorded data and, hence, so is its generalized inverse $(\mathbf{A}^T\mathbf{C}_d^{-1}\mathbf{A} + \mathbf{C}_m^{-1})^{-1}\mathbf{A}^T\mathbf{C}_d^{-1}$ (equation 11). Consequently, this generalized inverse matrix can be computed prior to acquisition; the equalization procedure in the field then requires only the computation of a matrix-vector multiplication (equation 11). This is an important difference with respect to surface-consistent deconvolution methods (Taner and Koehler, 1981; Levin, 1989; Cambois and Stoffa, 1992; Cary and Lorentz, 1993). The proposed deconvolution procedure is essentially a preprocessing step that can be applied in real time and to the complete seismogram.

Since the newly developed method is applicable to the complete seismic trace, this method is also suitable for multicomponent data. Application to multicomponent data is especially interesting because the quality of shear data recorded on the horizontal components is often more severely affected by receiver coupling effects than vertical component data (Krohn, 1984; Garotta, 2000). Besides, compensating multicomponent data for acquisition-related perturbations is important because these distort the characteristics of the vector wavefield; coupling has a different effect on horizontal and vertical receiver components (Krohn, 1984). This coupling can bias the observed polarization (Li and MacBeth, 1997; Michaud and Snieder, 2004). For example, determining the polarization direction of the leading split shear wave involves simultaneous rotation of the horizontal source and receiver coordinates to conform with the principal axes of an azimuthally anisotropic medium (Alford, 1986). In principle, application of reciprocity to multicomponent recordings also requires repeated experiments with horizontal and vertical vibrators (van Vossen, 2005) — thus, 3C × 3C recordings. However, the results on our field data indicate that small deviations from reciprocal conditions are allowed. In the field experiment, a pattern of explosive sources was used, and we consider the vertical component of the recorded wavefield. Therefore, it is worthwhile to investigate if we can also compensate multicomponent recordings generated by a single-component source.

Finally, we expect that further improvements are still possible when source and especially receiver phase perturbations can be accounted for. We do not correct for phase changes because nonuniqueness problems related to cycle skips in phase decomposition are yet to be resolved.

CONCLUSION

We successfully applied a newly developed preprocessing technique based on reciprocity to compensate for source and receiver perturbations on field data acquired in Manistee County, Michigan. Both prestack and poststack data show a significant improvement in S/N ratio after deconvolution. The poststack data show that subsurface structures can be observed after the deconvolution procedure, whereas they cannot be identified without compensating for the source and receiver amplitude perturbations.

The new procedure is based on reciprocity of the medium response. The source and receiver corrections are determined optimizing the fit between normal and reciprocal traces. Thus, this deconvolution technique requires data acquisition in a geometry that allows the use of apparently redundant recordings of reciprocal traces to constrain the source and receiver perturbations. Such a geometry requires symmetric wavefield sampling, i.e., data acquisition using coincident source and receiver positions.

A fundamental difference with existing surface-consistent deconvolution methods is that those methods assume CMP gathering is valid and therefore performs best when ground roll and multiples are suppressed prior to the application. However, the performance of multichannel filter operations, which are commonly used to suppress ground roll and multiples, deteriorates in the presence of amplitude and phase perturbations. Therefore, these corrections should be applied in the early stages of the processing, preferably to single-sensor data prior to group forming. Our new deconvolution procedure satisfies these criteria since it is essentially a preprocessing technique and can be applied directly to the recorded data; it is applicable to the whole seismic trace. The poststack results obtained using the newly developed deconvolution procedure compare favorably to the results of conventional surface-consistent deconvolution methods, since these require initial data scaling to obtain acceptable results.

The source corrections are sensitive to changes in near-surface conditions, especially to the water-saturation level, whereas a correlation between near-surface conditions and receiver perturbations is not observed. The receiver corrections vary rapidly along the spread. This indicates that both source and receiver perturbations must be taken into account to compensate for acquisition effects properly. The observed receiver response variation with frequency cannot be explained with the classical damped-harmonic oscillator model using only one resonant frequency. For frequencies below 100 Hz, the retrieved corrections are much larger than predicted by this model. In addition, ratios between theoretical damped-harmonic oscillator curves have one bounded minimum and maximum value, whereas we obtain ratios with two distinct minima or maxima.

ACKNOWLEDGMENTS

The authors wish to thank Schlumberger for funding this research and WesternGeco for allowing us to use the data. They further thank Ed Kragh, Jim Gaiser, Eric Verschuur, Bibi Ariman, and two anonymous reviewers for their constructive suggestions and Stefan Carpentier for assisting with the data processing.

APPENDIX A

STRUCTURE OF THE SYSTEM OF EQUATIONS

In this section, we illustrate the structure of the data vector $\mathbf{d}(\omega)$, the model vector $\mathbf{m}(\omega)$, and the coefficient matrix $\mathbf{A}$. We adopt the matrix-vector notation

$$\mathbf{d}(\omega) = \mathbf{A}\mathbf{m}(\omega) \tag{A-1}$$

to analyze the constraints on $\mathbf{m}(\omega)$ given by the convolutional model and reciprocity. Here, we give the expressions for $\mathbf{d}(\omega)$, $\mathbf{m}(\omega)$, and $\mathbf{A}$ for a configuration with two coincident source and receiver positions. It is straightforward to generalize the obtained expressions for N coincident source-receiver positions.

We denote the data generated by the ith source and the jth receiver with V_{ij}, the source term of the ith source with S_i, and the receiver term of the jth receiver with R_j. Then, the data vector $\mathbf{d}$ can be written as

$$\mathbf{d} = (V_{11} \quad V_{12} \quad V_{21} \quad V_{22})^T, \tag{A-2}$$

where T is the transpose operator. We order the unknown terms in the model vector according to

$$\mathbf{m} = (G_{11} \quad G_{12} \quad G_{22}|R_1 \quad R_2|S_1 \quad S_2)^T. \tag{A-3}$$

Note that reciprocity is used to reduce the number of unknown Green's functions explicitly: G_{ij} not only denotes the Green's function for data generated by the ith source and the jth receiver but also for the reversed source-receiver positions. Given the data and model vectors, the coefficient matrix reads

$$\mathbf{A} = \left(\begin{array}{ccc|c|c|cc} 1 & 0 & 0 & 1 & 0 & 1 & 0 \\ 0 & 1 & 0 & 0 & 1 & 1 & 0 \\ 0 & 1 & 0 & 1 & 0 & 0 & 1 \\ 0 & 0 & 1 & 0 & 1 & 0 & 1 \end{array}\right). \tag{A-4}$$

The vertical lines in this matrix indicate the separation between the columns corresponding to the medium-response terms, receiver terms, and source terms, respectively. The entries in $\mathbf{A}$ relate the data vector components to the unknown model components; they describe the decomposition of the data according to the convolutional model in the log/Fourier domain (equation 6).

APPENDIX B

REGULARIZATION: MINIMUM VARIATION CRITERION

Prior information on the medium response can be obtained by requiring that variation across common-offset sections of the medium response is small. The underlying idea is that lateral source and receiver variations result in amplitude variations in common-offset sections. If we correctly retrieve the lateral source and receiver variations and correct the recorded data for these source and receiver effects, the amplitude variations in these common-offset sections of the medium response are reduced to the minimum required by the data. We define variation in the common-offset medium response using a measure of length (Menke, 1984):

$$\begin{aligned} L(\mathbf{x}_o) &= [\mathbf{m}_G(\mathbf{x}_o) - \mu_G(\mathbf{x}_o)]^T [\mathbf{m}_G(\mathbf{x}_o) - \mu_G(\mathbf{x}_o)] \\ &= [\mathbf{A}_l(\mathbf{x}_o)\mathbf{m}_G(\mathbf{x}_o)]^T [\mathbf{A}_l(\mathbf{x}_o)\mathbf{m}_G(\mathbf{x}_o)], \end{aligned} \tag{B-1}$$

where $\mathbf{m}_G(\mathbf{x}_o)$ denotes the partition of $\mathbf{m}_G$ with offset $\mathbf{x}_o$, and the elements of $\boldsymbol{\mu}_G(\mathbf{x}_o)$ are the average of $\mathbf{m}_G(\mathbf{x}_o)$:

$$[\mu_G(\mathbf{x}_o)]_j = \frac{\sum_{i=1}^{N(\mathbf{x}_o)} [m_G(\mathbf{x}_o)]_i}{N(\mathbf{x}_0)}, \qquad j = 1, \ldots, N(\mathbf{x}_o), \tag{B-2}$$

with $N(\mathbf{x}_o)$ the number of traces with offset $\mathbf{x}_o$. The matrix $\mathbf{A}_l(\mathbf{x}_o)$ is the coefficient matrix and is defined such that $\mathbf{A}_l(\mathbf{x}_o)\mathbf{m}_G(\mathbf{x}_0) = \mathbf{m}_G(\mathbf{x}_o) - \mu_G(\mathbf{x}_o)$.

We define the minimum variation cost function L by combining all common-offset sections, using the number of traces in each common-offset section as weights, i.e., this criterion provides more reliable information using common-offset sections with many traces since the mean and variation with respect to this mean can be determined more accurately. The cost function L is given by

$$L = \sum_{\mathbf{x}_o} N(\mathbf{x}_o) L(\mathbf{x}_o) = [\mathbf{A}_l \mathbf{m}_G]^T \mathbf{W}_m [\mathbf{A}_l \mathbf{m}_G]. \quad \text{(B-3)}$$

The coefficient matrix $\mathbf{A}_l$ comprises all individual matrices $\mathbf{A}_l(\mathbf{x}_o)$, and the diagonal matrix $\mathbf{W}_m$ contains the corresponding weighting factors $N(\mathbf{x}_0)$, normalized such that the maximum value is

$$\max \left[\mathbf{A}_l^T \mathbf{W}_m \mathbf{A}_l\right] = \frac{2}{N+1}. \quad \text{(B-4)}$$

This maximum is set equal to the ratio of the number of unknowns in $\mathbf{m}_R$ or $\mathbf{m}_S$ over $\mathbf{m}_G$. The normalization reduces the dependency of the damping parameters on the number of sources/receivers.

The minimum variation criterion can be included in the inverse problem (equation 9), with the inverse of the medium-response model covariance given by

$$\mathbf{C}_{m_G}^{-1} = \mathbf{A}_l^T \mathbf{W}_m \mathbf{A}_l. \quad \text{(B-5)}$$

We set the prior medium response

$$\mathbf{m}_G^0 = \mathbf{0}. \quad \text{(B-6)}$$

The choice of the prior medium response does not influence the inversion results when these are set to a constant value. This criterion minimizes differences with respect to the average value in common-offset panels.

APPENDIX C

DAMPED HARMONIC OSCILLATOR

Both the internal mechanism for a geophone and the coupling phenomenon are thought to have a response characteristic of a damped harmonic oscillator. The complex normalized response of this model is (Krohn, 1984)

$$R(f) = \frac{-\left(\frac{f}{f_g}\right)^2 \left[1 + i\left(\frac{f}{f_c}\right)\eta_c\right]}{\left[1 - \left(\frac{f}{f_g}\right)^2 + i\left(\frac{f}{f_g}\right)\eta_g\right]\left[1 - \left(\frac{f}{f_c}\right)^2 + i\left(\frac{f}{f_c}\right)\eta_c\right]}. \quad \text{(C-1)}$$

In this model, f_g and f_c are the resonant frequencies and η_g and η_c are the damping factors. The subscript g refers to the geophone's internal spring, and c denotes the geophone-ground coupling. Critical damping occurs when η_g or $\eta_c = 2$.

REFERENCES

Alford, R. M., 1986, Shear data in the presence of azimuthal anisotropy: Dilley, Texas: 56th Annual International Meeting, SEG, Expanded Abstracts, 476–479.

Aritman, B. C., 2001, Repeatability study of seismic source signatures: Geophysics, **66**, 1811–1817.

Berni, A. J., and W. L. Roever, 1989, Field array performance: Theoretical study of spatially correlated variations in amplitude coupling and static shift and case study in the Paris basin: Geophysics, **54**, 451–459.

Blacquière, G., and L. Ongkiehong, 2000, Single sensor recording: Anti-alias filtering, perturbations and dynamic range: 70th Annual International Meeting, SEG, Expanded Abstracts, 33–36.

Cambois, G., and P. L. Stoffa, 1992, Surface-consistent deconvolution in the log/Fourier domain: Geophysics, **57**, 823–840.

Cary, P. W., and G. A. Lorentz, 1993, Four-component surface-consistent deconvolution: Geophysics, **58**, 383–392.

Castagna, J. P., and M. M. Backus, 1993, Offset-dependent reflectivity — Theory and practice of AVO analysis: SEG.

Fenati, D., and F. Rocca, 1984, Seismic reciprocity field tests from the Italian Peninsula: Geophysics, **49**, 1690–1700.

Garotta, R., 2000, Shear waves from acquisition to interpretation: SEG.

Hoover, G. M., and J. T. O'Brien, 1980, The influence of the planted geophone on seismic land data: Geophysics, **45**, 1239–1253.

Karrenbach, M., 1994, Multicomponent source equalization: 64th Annual International Meeting, SEG, Expanded Abstracts, 1449–1452.

Kelamis, P. G., and D. J. Verschuur, 2000, Surface-related multiple elimination on land seismic data — Strategies via case studies: Geophysics, **65**, 719–734.

Knopoff, L., and A. F. Gangi, 1959, Seismic reciprocity: Geophysics, **24**, 681–691.

Krohn, C. E., 1984, Geophone ground coupling: Geophysics, **49**, 722–731.

Levin, S. A., 1989, Surface-consistent deconvolution: Geophysics, **54**, 1123–1133.

Li, X., and C. MacBeth, 1997, Data-matrix asymmetry and polarization changes from multicomponent surface seismics: Geophysics, **62**, 630–643.

Luo, H., and Y. Li, 1998, The application of blind channel identification techniques to prestack seismic deconvolution: Proceedings of the IEEE, **86**, 2082–2089.

Menke, W., 1984, Geophysical data analysis: Discrete inverse theory: Academic Press.

Michaud, G., and R. Snieder, 2004, Error in shear-wave polarization and time splitting: Geophysical Prospecting, **52**, 123–132.

Newman, P., and J. T. Mahoney, 1973, Patterns — With a pinch of salt: Geophysical Prospecting, **21**, 197–219.

Ongkiehong, L., 1988, A changing philosophy in seismic data acquisition: First Break, **6**, no. 9, 281–285.

Ongkiehong, L., and H. J. Askin, 1988, Towards the universal seismic acquisition technique: First Break, **6**, no. 2, 46–63.

Taner, M. T., and F. Koehler, 1981, Surface consistent corrections: Geophysics, **46**, 17–22.

Taner, M., F. Koehler, and R. Sheriff, 1979, Complex seismic trace analysis: Geophysics, **44**, 1041–1063.

Tarantola, A., 1987, Inverse problem theory: Elsevier Science Publ. Co., Inc.

van Vossen, R., 2005, Deconvolution of land seismic data for source and receiver characteristics and near-surface structure: Ph.D. thesis, Utrecht University.

Vermeer, G., 1991, Symmetric sampling: The Leading Edge, **10**, 21–27.

Yilmaz, O., 2001, Seismic data analysis I — Processing, inversion and interpretation of seismic data: SEG.

Yu, G., 1985, Offset-amplitude variation and controlled-amplitude processing: Geophysics, **50**, 2697–2708.